Unveiling Structural Integrity of Tunnel type - $Na_{0.44}MnO_2$ Cathode for Sodium Ion Battery

Sankalpita Chakrabarty [a,b†], ***Javeed Ahmad Dar*** [c†], ***Akanksha Joshi*** [a,b], ***Arad Paperni*** [a,b], ***Sarah Taragin*** [a,b], ***Ananya Maddegalla*** [a,b], ***Gopalakrishnan Sai Gautam*** [c*], ***Ayan Mukherjee*** [a,b*], ***Malachi Noked*** [a,b*]

[a] *Department of Chemistry, Bar Ilan University, Ramat Gan, Israel*

[b] *Bar-Ilan Institute of Nanotechnology and Advanced Materials, Ramat Gan, Israel*

[c] *Department of Materials Engineering, Indian Institute of Science, Bengaluru 560012, India*

E-mail: malachi.noked@biu.ac.il

Experimental:

Synthesis of $Na_{0.44}MnO_2$:

The P2 type $Na_{0.44}MnO_2$ was synthesized through a facile and scalable solid-state approach using high purity precursors. All the chemicals were acquired from Sigma Aldrich and used without further purification. Stochiometric amount of Na_2CO_3, and $MnCO_3$ is mixed well and pre calcined at 300°C @ 2 °min^{-1} for 8h. Upon cooled down to the room temperature the powder is well grinded to make pellets and undergo another sintering at 850°C @ 5 °min^{-1} for 9h in Platinum boat. All the processes are performed in ambient conditions.

Physical characterization:

Structural characterization is employed using Bruker D8 Advanced X-ray diffractometer using Cu Kα radiation (λ=1.5414Å) within the 2θ range from 10° to 50°. The data were fitted with the Rietveld refinement method using MAUD software[1,2]. The refinement was performed using

the orthorhombic structure with a $Pbam$ space group, considering the lattice constants, a = 9.1Å, b = 26.34Å, and c = 2.82Å. The morphological analysis was studied by high resolution scanning electron microscope (HRSEM, FEI, Magellan 400 L) at the voltage of 5kV and current of 0.4 nA. The high-resolution transmission electron micrograph (HRTEM, JEM 32100, JEOL, accelerating voltage of 200kV, Gatan USC 4000 4x4k camera) of coated sample was recorded on lacey carbon-coated Cu gride. The elemental composition of the synthesized materials was investigated by Inductively coupled plasma atomic emission spectrometry (ICP-AES) technique with an Ultima-2 spectrometer (JobinYvon Horiba). The oxidation states of the various elements in each sample were measured using X-ray photoelectron spectroscopy (XPS, Thermo Scientific Nexsa soecro spectrometer).

Electrochemical study:

Electrode preparation: For making the slurry, the active material, Super P carbon black (Sigma Aldrich) and 10 % of poly-vinylidene fluoride (PVDF, Sigma Aldrich) binder in N-methyl-2-2pyrrolidone (NMP, Sigma Aldrich) is taken in 80:10:10 ratio and mixed in a Thinky mixer. The slurry was coated on a clean and polished Al foil using Doctor blade at thickness of 150 µm and dried for overnight at 100°C. After rolling, 12 mm of the electrode was punched, measured the weight, and kept overnight under dynamic vacuum at 120°C to avoid moisture.

Electrochemical test: The electrochemical study is conducted in a two-electrode cells configuration using coin-type cells (CR2032) in which Na metal (14 mm) is used as both counter and reference electrode. 1M $NaClO_4$/Ethylene carbonate (EC)/Diethylene carbonate (DEC) in 4:6 ratio is used as electrolyte solution. A total of 80 µl electrolyte solution is preserved with two Glass fiber separator (19mm) between working and Na electrode. The electrochemical measurements are performed in Bio-logic Science Instruments at 30°C in ambient condition. The galvanostatic discharge-charge cycling is recorded within the potential

window of 1.7 V to 4.0 V at CC-CV mode and the rate currents are normalized by active mass of the working electrode for each material.

Computational Methods:

Candidate structures

We took the disordered-$Na_{0.44}MnO_2$ structure, as obtained from the experimental X-ray diffraction refinement and enumerated the possible symmetrically-distinct Na-vacancy configurations by using the pymatgen package[3]. In total, we generated 647 unique configurations and took the 20 structures with the lowest electrostatic energies (computed via Ewald summations)[4] for further density functional theory (DFT)[5,6] calculations to identify the ground state Na-vacancy ordering. We followed a similar procedure for finding the ground state structure of $Na_{0.22}MnO_2$, where we generated 476 and 70 unique Na-vacancy configurations by using the original, disordered-$Na_{0.44}MnO_2$ structure, and the DFT-identified ground state Na-vacancy configuration at $Na_{0.44}MnO_2$, respectively. Subsequently, we used a total of 20 lowest electrostatic energy configurations for performing DFT calculations, with 12 and 8 configurations taken from the 476 and 70 set of structures, respectively, to identify the ground state configuration. The DFT-calculated ground state Na-vacancy configurations at both the $Na_{0.44}MnO_2$ and $Na_{0.22}MnO_2$ compositions are displayed in Fig. S2.

We used a 1×1×3 supercell for the NEB calculations to minimize interactions with periodic images and introduced a Na vacancy at the $Na_{0.22}MnO_2$ composition to model each hop. The minimum energy path (MEP) was initialized by a linear interpolation comprising of seven images between the initial and final configurations with a spring constant of 5 eV $Å^{-1}$. For all NEB calculations, including relaxation of the initial and final images, we used the SCAN functional without any Hubbard U corrections, since SCAN yields more accurate E_m, on

average, across several systems[7]. We relaxed the initial and final images with the same convergence criteria as we had used for identifying ground state structures (see SI). We converged our NEBs till the force component perpendicular to the elastic band dropped below |0.05| eV Å^{-1}. For the NEB calculations, we used Γ-centered *k*-point meshes with density of 32 *k*-points per Å.

DFT Calculations

We performed all DFT calculations with the Vienna *ab initio* simulation package (VASP)[8,9], employing the projector-augmented-wave potentials[10] identical to our previous work[11,12]. We expanded the plane wave basis up to a kinetic energy cutoff of 520 eV and sampled the irreducible Brillouin zone with a Γ-centered *k*-point mesh, where the density of the mesh used was at least 32 *k*-points per Å. We relaxed the lattice vectors, cell shape, and cell volume of all structures until the total energies and atomic forces converged within 0.01 meV and |0.03| eV Å^{-1}, respectively. For all structure relaxation calculations, we used the Hubbard *U* corrected [13,14] strongly constrained and appropriately normed (SCAN)[15] functional (i.e., SCAN+*U*) to describe the electronic exchange and correlation, where we used a *U* value derived in previous works[12,16,17].

Results and discussions:

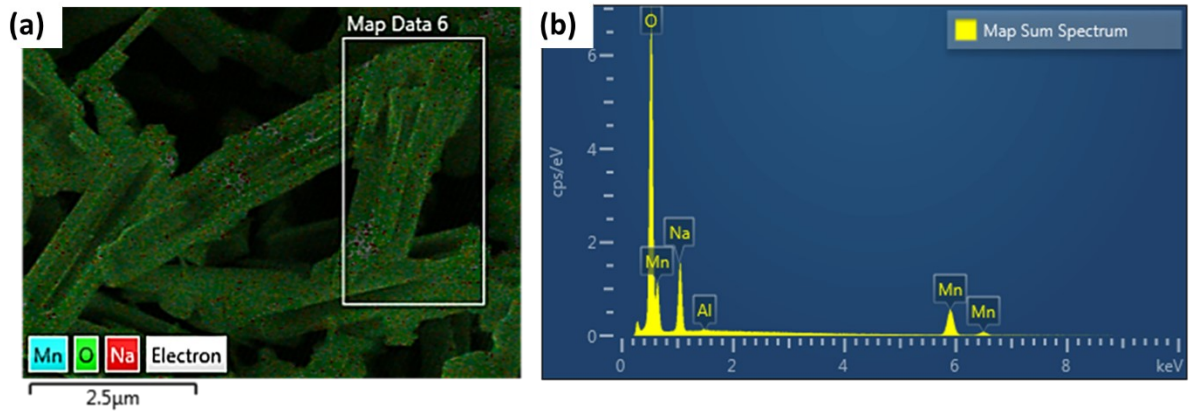

Figure S1: Elemental analysis by (a) EDS mapping and (b) corresponding spectra

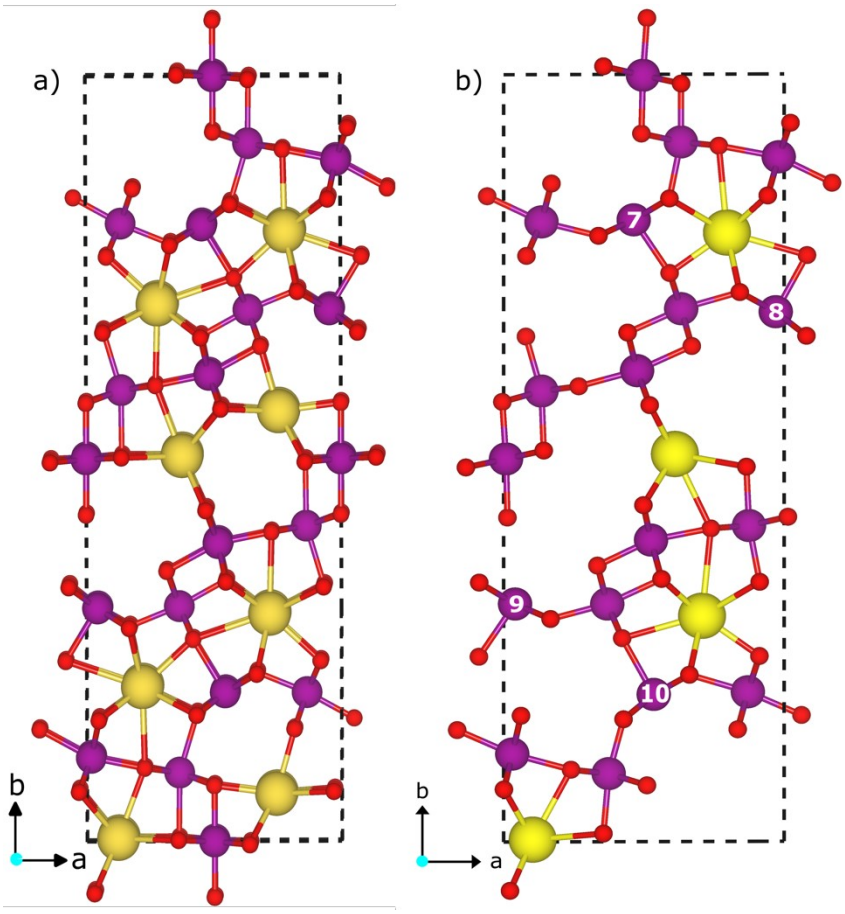

Figure S2. Structure of $Na_{0.44}MnO_2$ (a) and $Na_{0.22}MnO_2$ (b). Yellow, purple, and red spheres indicate Na, Mn and O atoms respectively. Mn atoms labelled from 7 to 10 have an oxidation state of +3 and exhibit square pyramidal coordination, while the other Mn atoms have an oxidation state of +4 and exhibit octahedral coordination.

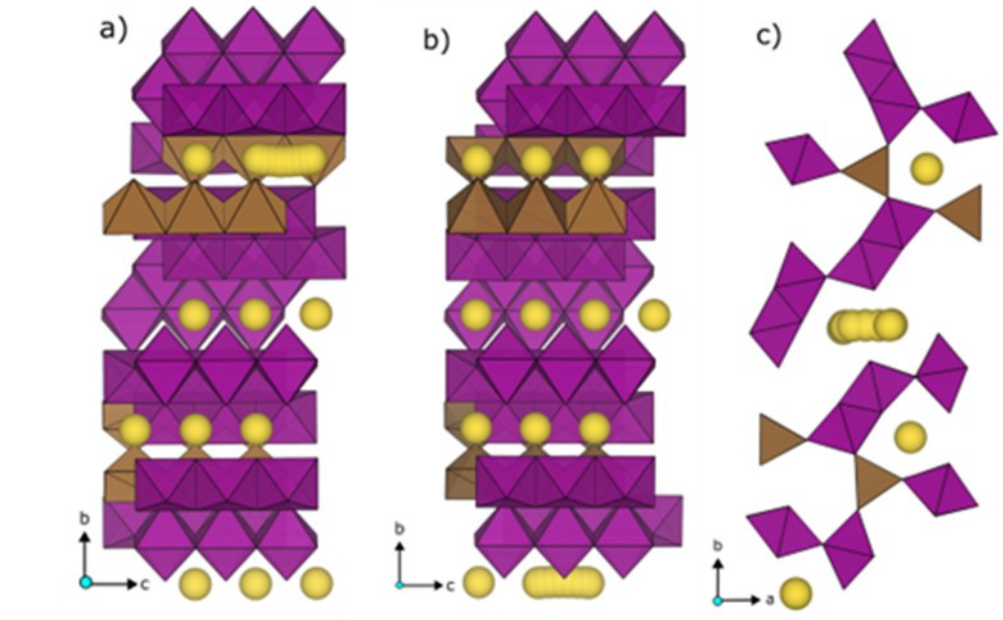

Figure S3. Calculated final minimum energy pathways traced by Na^+ in a) hop 1, b) hop 2, and c) hop 3. Note that hop 3 occurs diagonally across the Na tunnels in the $Na_{0.22}MnO_2$ structure. Purple and brown polyhedra signify MnO_6 octahedra and MnO_5 square pyramids.

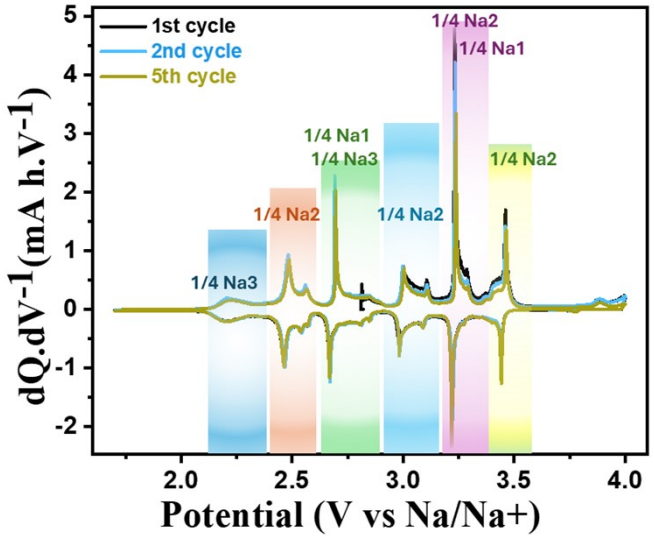

Figure S4. (a) Desodiation ordering of sodium ion within specific potential range

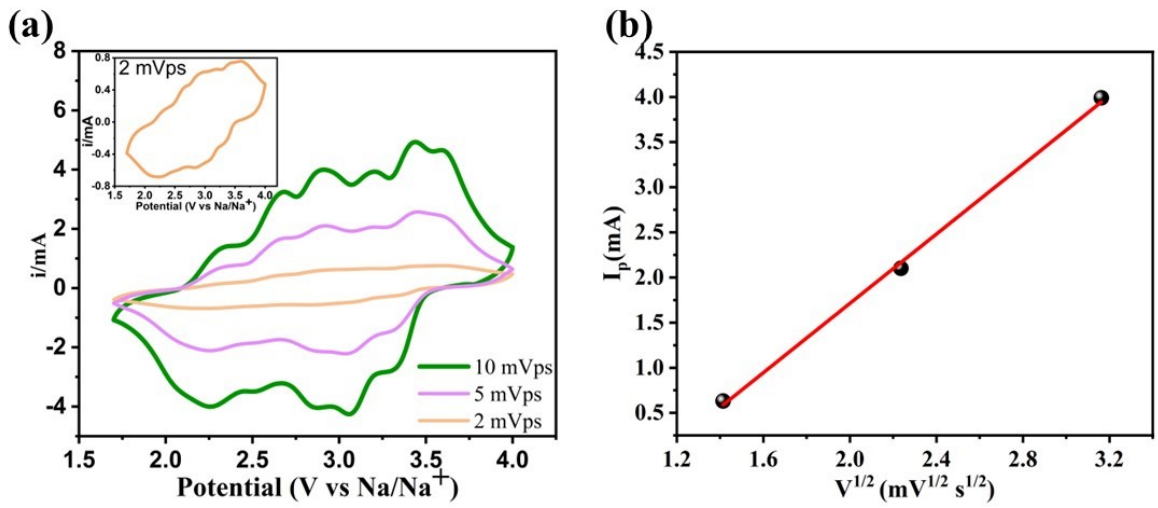

Figure S5. (a) Cyclic voltammetry at different sweep rate (b) plotting of peak current versus square root of scan rate

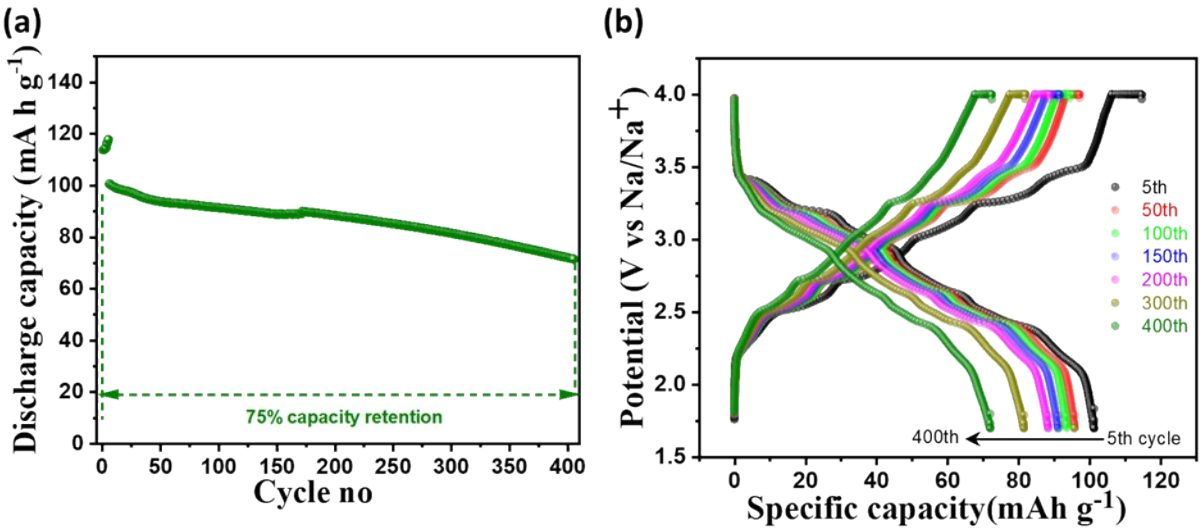

Figure S6. (a) Galvanostatic cycling stability and (b) voltage profile for different cycles at 0.5C rate

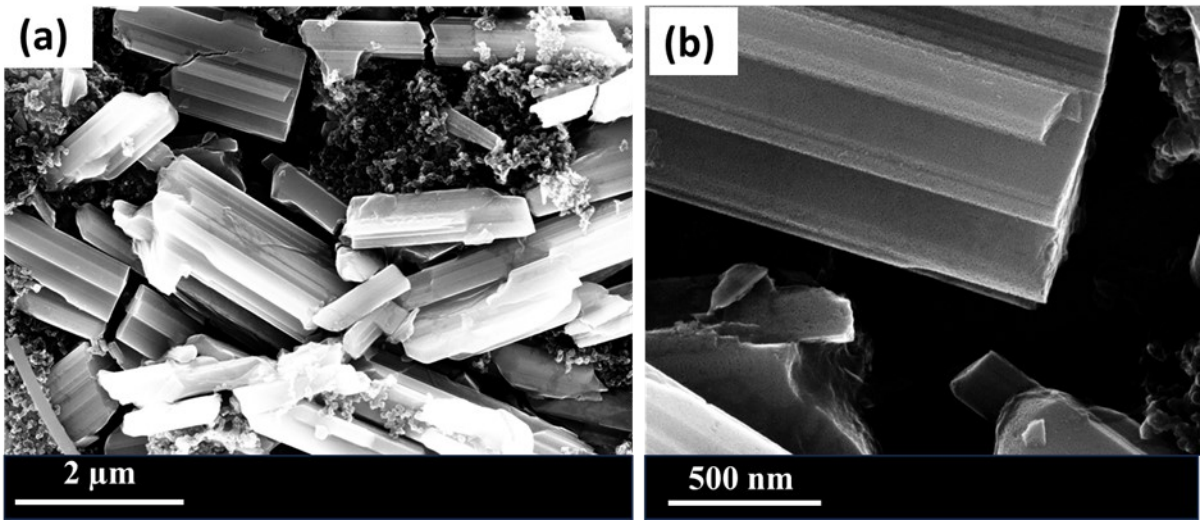

Figure S7. (a) HRSEM image of post-cycled cathode (b) magnified HRSEM image of selected area

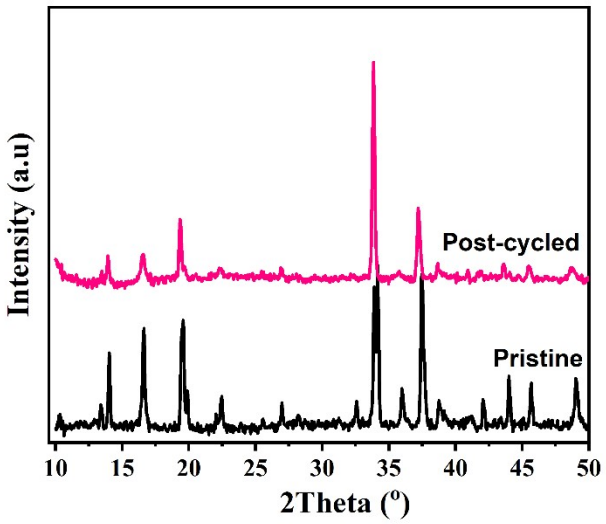

Figure S8. Post-cycled XRD pattern of tt-NMO cathode

Table S1:

Lattice parameters

a	b	c	alpha	beta	gamma
9.08 Å	26.31 Å	2.82 Å	90.0000	90.0000	90.0000
Unit-cell volume = 679.29 $Å^3$					
Rp = 2.87, R_{wp} = 3.73, χ^2 = 1.21, microstrain = 1.17 x 10^{-3}					

Table S2:

Structure parameters

	x	y	z	Site
1 Na1	0.17761	0.18581	0.00000	4g
2 Na2	0.65055	0.05407	0.50000	4h
3 Na3	0.14296	0.02245	0.00000	4g
4 Na4	0.75825	0.06976	0.00000	4g
5 Mn1	0.87734	0.18689	0.50000	4h
6 Mn2	0.50000	0.00000	0.00000	2c
7 Mn3	0.53304	0.19327	0.00000	4g

8 Mn4	0.34285	0.09096	0.50000	4h
9 Mn5	0.03137	0.10944	0.000	4g
10 O1	0.98445	0.05282	0.50000	4h
11 O2	0.86578	0.24351	0.00000	4g
12 O3	0.10043	0.18016	0.50000	4h
13 O4	0.50397	0.08076	0.00000	4g
14 O5	0.36135	0.09426	0.00000	4g
15 O6	0.35346	0.99635	0.50000	4h
16 O7	0.42031	0.17945	0.50000	4h
17 O8	0.66439	0.22054	0.50000	4h
18 O9	0.76091	0.11803	0.00000	4g

Table S3:

Bond length comparison between standard structure and this study:

Bond Length	Pbam	This study
Na1-O2	2.436	2.5344
Na1-O3	2.376	1.5837
Na1-O5	2.797	2.9429
Na1-O7	2.577	2.6234
Na1-O8	2.53	2.856
Na2-O4	2.36	2.0655
Na2-O6	2.381	3.1244
Na2-O1	2.452	2.524
Na3-O1	2.48	2.7029
Na3-O5	2.59	2.7355
Na3-O6	2.572	2.4754
Na4-O1	2.493	2.5332
Na4-O4	2.416	2.4675
Na4-O6	2.236	2.328
Na4-O9	2.314	1.2781
Mn1-O2	1.866	2.0623
Mn1-O3	1.902	2.0341
Mn1-O8	3.403	3.5375
Mn2-O4	1.919	2.1385
Mn2-O6	1.901	1.943
Mn3-O2	2.146	2.2606
Mn3-O7	1.892	1.7823
Mn4-O4	1.928	2.0516
Mn4-O5	1.887	1.425
Mn4-O7	3.538	2.4463
Mn5-O1	1.869	2.1032
Mn5-O3	1.943	2.4279
Mn5-O9	2.074	2.4670

Table S4. Calculated on-site magnetic moments and oxidation states of Mn atoms within the unit cell of $Na_{0.22}MnO_2$. The Mn sites with +3 oxidation states are labelled in **Figure S3** as well (i.e., Mn sites in square-pyramidal coordination).

Mn site	On-site magnetic moment (μ_B)	Oxidation state
1	3.06	4
2	3.05	4
3	3.05	4
4	3.05	4
5	3.06	4
6	3.06	4
7	3.81	3
8	3.81	3
9	3.81	3
10	3.81	3
11	3.01	4
12	3.01	4
13	3.01	4
14	3.01	4
15	2.98	4
16	2.96	4
17	2.98	4
18	2.96	4

Table S5: comparison between our material and reported literature.

Material	Voltage	1st charge capacity (mA h g-1)	1st discharge capacity (mA h g-1)	Capacity retention		Current rate	References
				200 cycles	400 cycles		
$Na_{0.44}MnO_2$	**1.7-4V**	**110**	**115**	**90%**	**75%**	**0.5C**	**This work**
$Na_{0.44}MnO_2$	2-4V	**38**	84	77% (100 cycle)		0.3C	[18]
$Na_{0.44}MnO_2$	2-3.8V	**54**	100	99.6% (2000 cycle)		8.3 C	[19]
$Na_{0.44}MnO_2$	2-4.2V	**60**	113	68% (500 cycle)		5C	[20]
AlPO4 coated $Na_{0.44}MnO_2$	2-4.2V	**60**	109	80% (500 cycle)		5C	
$Na_{0.44}MnO_2$	2-4.5V	**68**	94		70.3%	1C	[21]
1 wt% In2O3-coated $Na_{0.44}MnO_2$	2-4.5V	**40**	74		86.7%	1C	
$Na_{0.44}[Mn_{1-x}Ti_x]O_2$	1.5–3.9 V	**45-60**	100-110	Not mentioned			[22]
$Na_{0.44}MnO_2$	1.5–3.8 V	**Not mentioned**	120	86% (600 cycle)		5C	[23]
$Na_{0.44}MnO_2$ Nanowire	2–4 V	**66.7**	120.4	97.3% (200 cycle)		0.1C	[24]
$Na_{0.44}MnO_2$	2–3.8 V	**Less than 60**	115	75.7(200 cycle)		1C	[25]

References:

1 A. Mukherjee, S. Chakrabarty, S. Taragin, E. Evinstein, P. Bhanja, A. Joshi, H. Aviv, I. Perelshtein, M. Mohapatra, S. Basu and M. Noked, *Small*, 2024, **2308886**, 1–10.

2 L. Wang, A. Mukherjee, C. Y. Kuo, S. Chakrabarty, R. Yemini, A. A. Dameron, J. W. DuMont, S. H. Akella, A. Saha, S. Taragin, H. Aviv, D. Naveh, D. Sharon, T. S. Chan, H. J. Lin, J. F. Lee, C. Te Chen, B. Liu, X. Gao, S. Basu, Z. Hu, D. Aurbach, P. G. Bruce and M. Noked, *Nat. Nanotechnol.*, , DOI:10.1038/s41565-023-01519-8.

3 S. Ping, W. Davidson, A. Jain, G. Hautier, M. Kocher, S. Cholia, D. Gunter, V. L. Chevrier, K. A. Persson and G. Ceder, *Comput. Mater. Sci.*, 2013, **68**, 314–319.

4 P. P. Ewald, *Ann. Phys.*, 1921, **369**, 253–287.

5 J. Y. Jung, J. H. Park, Y. J. Jeong, K. H. Yang, N. K. Choi, S. H. Kim and W. J. Kim, *Korean J. Physiol. Pharmacol.*, 2006, **10**, 289–295.

6 C. H. Chu and C. W. Leung, *Integr. Equations Oper. Theory*, 2001, **40**, 391–402.

7 R. Devi, B. Singh, P. Canepa and G. Sai Gautam, *npj Comput. Mater.*, 2022, **8**, 1–13.

8 G. Kresse and J. Furthmüller, *Phys. Rev. B - Condens. Matter Mater. Phys.*, 1996, **54**, 11169–11186.

9 G. Kresse and J. Hafner, *Phys. Rev. B*, 1993, **47**, 558–561.

10 G. Kresse and D. Joubert, *Phys. Rev. B - Condens. Matter Mater. Phys.*, 1999, **59**, 1758–1775.

11 B. Patra, K. Kumar, D. Deb, S. Ghosh, G. S. Gautam and P. Senguttuvan, *J. Mater. Chem. A*, 2023, **11**, 8173–8183.

12 S. Swathilakshmi, R. Devi and G. Sai Gautam, *J. Chem. Theory Comput.*, 2023, **19**, 4202–4215.

13 S. Dudarev and G. Botton, *Phys. Rev. B - Condens. Matter Mater. Phys.*, 1998, **57**,

1505–1509.

14 V. I. Anisimov, J. Zaanen and O. K. Andersen, *Phys. Rev. B*, 1991, **44**, 943–954.

15 J. Sun, A. Ruzsinszky and J. Perdew, *Phys. Rev. Lett.*, 2015, **115**, 1–6.

16 O. Y. Long, G. Sai Gautam and E. A. Carter, *Phys. Rev. Mater.*, 2020, **4**, 1–15.

17 G. Sai Gautam and E. A. Carter, *Phys. Rev. Mater.*, 2018, **2**, 1–14.

18 E. Oz, S. Altin and S. Avci, *ACS Omega*, 2023, **8**, 27170–27178.

19 Q. Liu, Z. Hu, M. Chen, Q. Gu, Y. Dou, Z. Sun, S. Chou and S. X. Dou, *ACS Appl. Mater. Interfaces*, 2017, **9**, 3644–3652.

20 Z. Zhao, X. Huang, Y. Shao, S. Xu, L. Chen, L. Shi, Q. Yi, C. Shang and D. Zhang, *Chem. Eng. J. Adv.*, 2022, **10**, 100292.

21 W. Liu, Q. Ren, M. Yang, L. Liu, Y. Zhang, D. Su, J. Wen, Q. Wang, X. Wang and Y. Feng, *J. Alloys Compd.*, 2022, **896**, 163087.

22 Y. Wang, J. Liu, B. Lee, R. Qiao, Z. Yang, S. Xu, X. Yu, L. Gu, Y. S. Hu, W. Yang, K. Kang, H. Li, X. Q. Yang, L. Chen and X. Huang, *Nat. Commun.*, , DOI:10.1038/ncomms7401.

23 M. S. Chae, H. J. Kim, H. Bu, J. Lyoo, R. Attias, B. Dlugatch, M. Oliel, Y. Gofer, S. T. Hong and D. Aurbach, *Adv. Energy Mater.*, 2020, **10**, 1–7.

24 Y. Liu, X. Liu, F. Bu, X. Zhao, L. Wang, Q. Shen, J. Zhang, N. Zhang, L. Jiao and L. Z. Fan, *Electrochim. Acta*, 2019, **313**, 122–130.

25 C. Ferrara, C. Tealdi, V. Dall'asta, D. Buchholz, L. G. Chagas, E. Quartarone, V. Berbenni and S. Passerini, *Batteries*, , DOI:10.3390/batteries4010008.